Accurate determination of parameters of a claw pole motor with SMC stator core by finite element magnetic field analysis

Y.G. Guo[1], J.G. Zhu[1], and H.Y. Lu[2]

[1]Faculty of Engineering, University of Technology, Sydney, P.O. Box 123, NSW 2007, Australia

[2]Faculty of Information Technology, University of Technology, Sydney, P.O. Box 123, NSW 2007, Australia

E-mail: youguang@eng.uts.edu.au, joe@eng.uts.edu.au, helenlu@it.uts.edu.au

Abstract

Effective and accurate prediction of key motor parameters, such as winding flux, back electromotive force, inductance and core losses, is crucial for design of high performance motors. Particularly, for electrical machines with new materials and non-conventional topology, traditional design approaches based on the equivalent magnetic circuit, empirical formulae and previous experiences cannot provide correct computation. This paper presents accurate determination of major parameters of a three-phase three-stack claw pole permanent magnet motor with soft magnetic composite (SMC) stator core by finite element analysis of magnetic field. The effects of magnetic saturation and armature reaction are considered. The theoretical results by numerical analysis are validated by the experiments on the claw pole SMC motor prototype.

Keywords: Armature reaction; Claw pole motor; Core loss; Electromotive force; Finite element analysis; Inductance; Soft magnetic composite.

1. Introduction

Soft magnetic composite (SMC) materials and their application in electrical machines have attracted a strong interest of research in the past decade [1]. The unique properties of the

material include magnetic and thermal isotropy, extremely low eddy current loss and relatively low total core loss at medium and higher frequencies, net-shape fabrication process (no need of further machining), and the prospect of very low cost mass production [2]. The basis for the material is the bonded iron powder of high purity and high compressibility. The powder particles are bonded with a coating, which produces electrical insulation between particles. The coated powder is then pressed into a solid material using a die and finally heat treated to anneal and cure the bond [3].

This type of material is in general magnetically isotropic due to its powdered nature and this creates key design benefits for electromagnetic devices. The magnetic circuits can now be designed with three-dimensional (3D) flux path and radical topologies can be exploited to achieve high machine performance [2], because the magnetic field does not have to be constrained in a plane as that in laminated steels, which are commonly used in rotating electrical machines and transformers. Typical examples of SMC application are claw pole and transverse flux machines, in which the magnetic field is really 3D due to the complex structure of the machines [4].

In electrical machines with 3D magnetic flux, the **B** (flux density) locus at one location can be very complicated when the rotor rotates, such as one-dimensional (1D) alternating, two-dimensional (2D) or even 3D circularly or elliptically rotating, all with or without harmonics [5]. The locus patterns are affected by the magnetic saturation of the core, and are further distorted by the armature reaction when the motor operates at load. Different vector magnetisations have very different effects on the motor's parameters and performance such as core losses and therefore they should be carefully investigated and properly considered in

motor design and parameter computation.

This paper presents the calculation of major parameters of a three-phase three-stack permanent magnet (PM) claw pole motor with SMC stator core based on 3D magnetic field finite element analysis (FEA), including the winding flux, back electromotive force (*emf*), inductance and core losses. The effects of magnetic saturation of the core and armature reaction are taken into account. The theoretical computation is verified by the experimental results on the prototype motor.

2. Claw Pole SMC Motor Prototype

To investigate the application potential of SMC materials in electrical machines, a three-phase three-sack claw pole motor with SMC stator core has been designed, fabricated and tested [6]. Fig. 1 illustrates the magnetically relevant parts of the motor and Table I lists the major dimensions and performance. Three arrays of NdFeB PMs are mounted on the inner surface of the rotor yoke, which is made of mild steel considering the magnetic field in it is almost constant. The three phases of the inner stator are stacked axially and are shifted to each other by 120° electrical. The core of each phase consists of two claw pole discs of SMC, which are modelled in a die. The motor has successfully operated with a sensorless brushless DC drive, delivering an output of 500 W at 1800 r/min.

3. FEA of Magnetic Field

In a claw pole motor, the magnetic field is really 3D due to the complex structure. The conventional approach based on the magnetic circuit cannot provide accurate calculation of

the magnetic field distribution, as well as the motor's parameters and performance. This is particularly true for machines with new topology and new materials, because there is little previous experience and empirical data.

For design and analysis of a claw pole motor, modern numerical techniques, e.g. FEA, proves to be a powerful computational tool, which can consider the non-linearity of the magnetic materials and the structural and dimensional details. In this paper, the major parameters of the motor are computed based on the magnetic field distribution, which is obtained by 3D FEA. As there is very little eddy current effect in the SMC core, magnetostatic analysis is conducted [7].

Considering the symmetry of the structure and the almost independent magnetic circuits between the three stacks, only one pole of one phase is required for the FEA of magnetic field, as shown in Fig. 2.

At the two radial boundary planes of one pole pitch, the magnetic scalar potential obeys the so-called half-periodical boundary conditions:

$$\varphi_m\left(r, \Delta\theta/2, z\right) = -\varphi_m\left(r, -\Delta\theta/2, -z\right) \tag{1}$$

where $\Delta\theta = 18^\circ$ is the angle of one pole pitch. The origin of the cylindrical coordinate system is located at the centre of the stack. The conditions of magnetic flux density are given by

$$B_{r,\theta}\left(r, \Delta\theta/2, z\right) = -B_{r,\theta}\left(r, -\Delta\theta/2, -z\right) \tag{2}$$

$$B_z\left(r, \Delta\theta/2, z\right) = B_z\left(r, -\Delta\theta/2, -z\right) \tag{3}$$

4. Winding Flux and Back *emf*

4.1 PM flux and back *emf* of stator winding

PM flux, defined as the flux of a phase winding produced by the rotor PMs, can be obtained from the no-load magnetic field distribution, which is solved by FEA. Fig. 3 shows the flux density vector plots at no-load, with line length is proportional to the magnitude. It can be seen that the major path of the magnetic flux of the PMs is along one of the PMs − the main air gap − one of the SMC claw pole stator core pieces − the SMC stator yoke − another SMC claw pole stator core piece − main air gap − another PM and then − the mild steel rotor yoke to form a closed loop. There is also a considerable amount of leakage flux through the gaps between the side and end surfaces of the claw poles of the two separated discs. Both the main flux and leakage flux are 3D.

The winding flux can be computed by the surface integral of flux density $\boldsymbol{B}$ after the magnetic field distribution is solved by FEA. For this claw pole motor, the computation is based on the middle cross-sectional area of the stator yoke, marked as A-A in Fig. 3.

As the rotor rotates, the PM flux varies and an *emf* is induced. The *emf* frequency depends on the rotor speed, while the *emf* waveform is determined by the waveform of the flux. At no load, the flux waveform was calculated by rotating the rotor magnets for one pole pitch in 12 steps. As plotted in Fig. 4, this flux waveform is almost perfectly sinusoidal versus the rotor position. The maximum value of the flux is 0.480 mWb.

The induced winding *emf*, by differentiating the PM flux with respect to time, is given by

$$E_1 = \frac{\omega_1 N_1 \phi_1}{\sqrt{2}} \tag{4}$$

where $\omega_1 = 2\pi f_1$ is the angular rotor speed in electrical radians per second, f_1 the frequency of the induced stator *emf* in Hz, N_1 the number of turns of the stator winding, and ϕ_1 the magnitude of the PM flux. The rms value of *emf* is calculated as 48.0 V at 300 Hz.

4.2 PM flux at load

At load, the stator current will produce a magnetic field to interact with the PM flux. The effect of the armature reaction by the stator current is not difficult to analyse if the magnetic circuit is linear, but it becomes complicated when the core material is saturated, increasing the reluctance of the magnetic circuit and deviating the motor performance [8]. Fig. 5 plots the flux density vectors generated by the rated stator current only, showing that the major flux path of armature reaction is different from that of the PM flux.

The FEAs are performed at no-load, half-load, and full-load, respectively, and the curves of PM flux versus the rotor angular position are shown in Fig. 4. To consider the effect of saturation, firstly the non-linear analysis is conducted with the excitations of both PMs and armature current i_1, and the permeability of each element is saved. Then with the saved permeabilities, a linear analysis is conducted under the excitation of the PMs only so that the PM flux can be obtained. Under the condition of the optimum BLDC control, the stator current is in phase with the back *emf*, i.e. lagging the PM flux by 90$^{\mathrm{o}}$ electrical. The fundamental of the stator current can be determined by

$$i_1 = \sqrt{2}I_{1rms} \sin\theta \tag{5}$$

where I_{1rms} is the *rms* value of the stator current (4.1A for full-load), θ is the rotor angle with the zero position where the claw poles line up with the rotor PMs, as shown in Fig. 2.

The fundamental component of the stator flux produced by PMs at no-load is 0.480 mWb, decreasing to 0.476 mWb at half-load, and 0.464 mWb at full-load. The reduction of the PM flux due to armature reaction is 0.002 mWb/A from no-load to half-load, and 0.006 mWb/A from half-load to full-load. The flux reduction is not linear with the stator current but increases drastically with the current. The loss of the flux fundamental, the back *emf* and developed torque at full-load due to armature reaction is about 3.3%.

5. Calculation of Winding Inductance

5.1 Secant inductance

The winding inductance is one of the key parameters determining the motor's performance. As the magnetic circuit of each phase is almost independent, the mutual inductance between phase windings can be considered as zero. The self inductance of each phase is usually computed by the flux-linkage method as

$$L = \frac{\lambda}{i} = \frac{N\phi}{i} \tag{6}$$

or the magnetic energy method as

$$L = \frac{2W_f}{i^2} \tag{7}$$

where λ, ϕ and W_f are the magnitudes of the flux-linkage and flux linking the winding, and the magnetic co-energy stored in the whole machine, respectively, produced by a current i in each of N turns.

A difficulty with the flux-linkage method is the accurate determination of the flux flowing through the stator winding. Theoretically, the flux can be computed by the surface integral of

flux density $\boldsymbol{B}$, or the loop integral of vector potential $\boldsymbol{A}$ after the magnetic field distribution is solved by FEA, but it is not easy to define a proper integration surface or path when the winding is not a simple loop or is of non-negligible size. For this claw pole motor, the winding flux can be approximately calculated based on the middle cross-sectional area of the stator yoke, marked as A-A in Fig. 5.

By contrast, the energy method can avoid the difficulty of choosing the proper integration geometry. It calculates the energy or co-energy stored in all the elements and is considered as quite accurate because the principle of FEA is based on the minimisation of magnetic field energy. In this paper, the investigation on the winding inductance is mainly carried out by the energy method.

To consider the saturation caused by both the stator current and PMs, the two-step analysis method is employed, i.e. a non-linear analysis with the excitations of both PMs and armature current i for saving the permeability of each element, and then a linear analysis with a stator current only and the saved permeabilities is performed to find the W_f in (7).

The calculated phase winding inductance (L_{sec}) versus different rotor angle and load is shown in Fig. 6. This calculation is in fact the secant (or apparent) inductance, i.e. the slope of the linearised characteristic of flux-linkage versus current through the origin and the operating point, as shown in Fig. 7.

5.2 Incremental inductance

The behaviour of an electric circuit is governed by the so-called incremental (or differential) inductance, along the tangential line at the operating point, as illustrated in Fig. 7. The governing equation of one phase winding circuit can be described as

$$u = Ri + \frac{d\lambda}{dt} \tag{8}$$

where u, R, i and λ are the voltage, resistance, current and flux linkage of the winding, respectively. The flux linkage, contributed by both the stator current and PMs, varies with stator current i and rotor position θ as

$$\lambda = \lambda(i, i_{m1}, i_{m2}, \cdots i_{mp}, \theta) \tag{9}$$

where i_{m1}, i_{m2}, …, i_{mp} are the currents of the equivalent coils of magnets, respectively, and p is the number of magnets of one stack. Substituting (9) into (8) and applying the chain rule of the flux linkage, the voltage can be expressed as

$$u = Ri + \frac{\partial \lambda}{\partial i} \frac{di}{dt} + \frac{\partial \lambda}{\partial \theta} \frac{d\theta}{dt} = Ri + L_{inc} \frac{di}{dt} + E \tag{10}$$

$$L_{inc} = \frac{\partial \lambda}{\partial i} \tag{11}$$

where L_{inc} is the incremental inductance, and E is the rotational *emf*. Note that the currents of the equivalent coils of magnets are constants, so their derivatives are zero.

The calculation of L_{inc} involves calculating the increment of flux-linkage due to a small perturbation of current. To avoid the difficulty in defining the integration geometry for flux-linkage computation, the incremental energy method (IEM) is often used [9, 10]. IEM computes the inductance using the magnetic field FEA in conjunction with energy/current perturbation.

For a lossless (conservative) magnetic system, the sum of magnetic energy W and co-energy W_c is given by

$$W + W_c = \lambda i + \lambda_{m1} i_{m1} + \lambda_{m2} i_{m2} + \cdots + \lambda_{mp} i_{mp} \tag{12}$$

By differentiating the both sides of the above equation, the follows can be obtained

$$
\begin{aligned}
dW + dW_c = {} & id\lambda + \lambda di \\
& + i_{m1} d\lambda_{m1} + i_{m2} d\lambda_{m2} + \cdots + i_{mp} d\lambda_{mp} \\
& + \lambda_{m1} di_{m1} + \lambda_{m2} di_{m2} + \cdots + \lambda_{mp} di_{mp}
\end{aligned}
\tag{13}
$$

or

$$dW = id\lambda + i_{m1} d\lambda_{m1} + i_{m2} d\lambda_{m2} + \cdots + i_{mp} d\lambda_{mp} \tag{14a}$$

$$dW_c = \lambda di + \lambda_{m1} di_{m1} + \lambda_{m2} di_{m2} + \cdots + \lambda_{mp} di_{mp} \tag{14b}$$

The differential of dW_c can also be expressed as

$$dW_c = \frac{\partial W_c}{\partial i} di + \frac{\partial W_c}{\partial i_{m1}} di_{m1} + \frac{\partial W_c}{\partial i_{m2}} di_{m2} + \cdots + \frac{\partial W_c}{\partial i_{mp}} di_{mp} \tag{15}$$

Comparing (14b) and (15) revels that

$$\lambda = \frac{\partial W_c}{\partial i} \tag{16}$$

Then, the incremental self-inductance formulation using the energy/current perturbation method can be written as

$$L_{inc} = \frac{\partial^2 W_c}{\partial i^2} \approx \frac{W_c(i + \Delta i) + W_c(i - \Delta i) - 2W_c(i)}{(\Delta i)^2} \tag{17}$$

This is the general IEM formula, proposed in [9, 10]. It seems that two incremental analyses are required for self-inductance (and even four for mutual ones) [11]. In fact, (17) can be reduced to a very simple form, requiring one incremental analysis only. For linear analysis,

the stator current i can be any value, e.g. 0. With a current perturbation Δi only (from zero current), this formula can be reduced to

$$L_{inc} \approx \frac{2\Delta W_c}{(\Delta i)^2} \tag{18}$$

where ΔW_c is the increment of magnetic co-energy, which equals the energy in the linear analysis.

In summary, the modified IEM (MIEM) calculates the incremental inductance by the following steps [12]: (I) Perform non-linear magnetic field analysis with the excitation of both the stator current and PMs; (II) Determine and save the differential permeability in each element; (III) Conduct linear analysis with the saved differential permeabilities and a perturbed current only; (IV) Calculate the co-energy increment and then the incremental inductance by (18). In fact, the perturbed current in (III) can be large since the magnetic field analysis is linear.

The MIEM is applied in this paper to compute the incremental inductance of the phase winding at different rotor positions and loads, as shown in Fig. 6. Comparing to the secant counterpart, the incremental inductance generally has smaller values and varies more drastically. This agrees with the slopes of the cord and tangential lines in Fig. 7.

6. Core Losses

Core loss prediction is a key issue in the design and optimisation of electrical machines. Unlike the laminated machines, SMC ones have comparable core loss to the copper loss. The core loss calculation can be very complex because in claw pole motors the flux density patterns are quite complicated, particularly when the armature reaction is taken into account.

A comprehensive method has been used for predicting the core losses in SMC machines with 3D flux paths [13]. Different formulations are applied for various flux density patterns as summarised in the follows:

The alternating core loss is calculated by

$$P_a = C_{ha} f B_P^{\ h} + C_{ea} (f B_P)^2 + C_{aa} (f B_P)^{1.5} \tag{19}$$

and the core loss with circular flux density pattern by

$$P_r = P_{hr} + C_{er} (f B_P)^2 + C_{ar} (f B_P)^{1.5} \tag{20}$$

where

$$\frac{P_{hr}}{f} = a_1 \left[\frac{1/s}{(a_2 + 1/s)^2 + a_3^2} - \frac{1/(2-s)}{[a_2 + 1/(2-s)]^2 + a_3^2} \right], \quad s = 1 - \frac{B_P}{B_s} \sqrt{1 - \frac{1}{a_2^2 + a_3^2}} \ .$$

The coefficients C_{ha}, h, C_{ea}, C_{aa}, C_{er}, C_{ar}, a_1, a_2, a_3, and B_s can be obtained from the measured core losses on the SMC sample under various frequencies, f, and various peak flux densities, B_p by the curve fitting technique [5, 13].

The core loss with elliptical B is predicted from the alternating and circularly rotating core losses by

$$P_t = R_B P_r + (1 - R_B)^2 P_a \tag{21}$$

where $R_B = B_{min}/B_{maj}$ is the axis ratio, B_{maj} and B_{min} are the major and minor axes of the elliptical B locus, and P_r and P_a are the core losses with a circular B with $B_{maj} = B_{min} = B_p$ and an alternating B with peak value B_p, respectively.

The core losses are computed based on elements. The B pattern in each element is obtained by the 3D magnetic field FEA. Fig. 8 plots the flux density loci at no-load, half-load and full-load in a typical element in the middle of the stator claw pole (Point C of Fig. 2).

The flux density loci are disturbed by the armature reaction. For any flux density locus of an element, the three components can always be expanded into Fourier series as

$$B_i(t) = \sum_{k=0}^{\infty} [B_{isk} \sin(2\pi k f t) + B_{ick} \cos(2\pi k f t)] \tag{22}$$

where $i = r, \theta, z, B_r, B_\theta$, and B_z are the radial, circumferential and axial components of $\boldsymbol{B}$, respectively. Each harmonic consists of two parts:

$$\mathbf{n_{sk}} \sqrt{B_{rsk}^2 + B_{\theta sk}^2 + B_{zsk}^2} \sin(2\pi k f t) \tag{23a}$$

$$\mathbf{n_{ck}} \sqrt{B_{rck}^2 + B_{\theta ck}^2 + B_{zck}^2} \cos(2\pi k f t) \tag{23b}$$

where $\boldsymbol{n_{sk}}$ and $\boldsymbol{n_{ck}}$ are the unit vectors, determined by B_{rsk}, $B_{\theta sk}$ and B_{zsk}, and B_{rck}, $B_{\theta ck}$ and B_{zck}, respectively. The two parts generally form an elliptical trajectory in a plane determined by $\boldsymbol{n_{sk}}$ and $\boldsymbol{n_{ck}}$. The major axis B_{kmaj} and the minor axis B_{kmin} can be obtained by a coordinate rotation for the standard equation.

For each elliptically rotating flux density harmonic, the loss can be predicted from the corresponding alternating and rotational losses according to the axis ratio of the elliptical flux density [14]. For each element, the core loss can be obtained by summing up the contributions from the flux density harmonics, which can be derived from the Poynting's theorem [13]. Therefore, the total loss is

$$P_t = \sum_{e=1}^{Ne} \sum_{k=0}^{\infty} \left[P_{rk} R_{BK} + (1 - R_{BK})^2 P_{ak} \right] \tag{24}$$

where N_e is the number of elements of the core, $R_{BK} = B_{kmin}/B_{kmaj}$ is the axis ratio of the k-th harmonic flux density, P_{rk} is the purely rotational loss with flux density B_{kmaj}, and P_{ak} is the alternating loss with $B_p = B_{kmaj}$.

The core loss is calculated as 58.0 W at no-load, but goes up to 67.4 W at half-load, and further to 81.8 W at full-load. The core loss increment is non-linearly related to the armature reaction, e.g. 4.6 W/A from no-load to half-load, and 7.0 W/A from half-load to full-load.

7. Experimental Validation

7.1 Winding flux and back *emf*

To validate the calculation of the winding flux and back *emf*, the open-circuit voltage is measured by a CRO when the prototype is driven by a DC motor. Fig. 9 shows the measured *emf* waveforms at 1800 r/min or 300 Hz, which are very close to sinusoidal. The waveforms of the three phase *emf*s are with the same magnitude but shifted each other by 120° electrical in phase angles. It can be seen that the magnitude of the phase *emf* is about 68 V, corresponding to 48.1 V of rms value, or 0.481 mWb flux of phase winding. These values agree well with the computations in Section 4.1.

7.2 Inductance measurement

For measurement of the inductance, a small AC current (0.2 A, 500 Hz) was fed into the phase winding when the rotor is locked. The voltage across the two terminals, V_1, and the current flowing through the winding, I_1, are measured. The phase winding inductance can be calculated by

$$L_1 = \sqrt{(V_1 / I_1)^2 - R_1^{\,2}} \, / (2\pi f_1) \tag{25}$$

where f_1 is the frequency, and R_1 is the resistance of the phase winding. The inductances are measured at different rotor positions, as shown in Fig. 10. For comparison, the computed secant and incremental inductances at no-load are also shown in the figure, where L_{sec} and L_{inc} are computed secant and incremental inductances, respectively, and L_{mea} is the measured value. The computations agree with the measurements. Some error may be caused by the measuring current, which causes a small loop in the vicinity of the saturation point in the B-H curve. Another possible reason is the eddy current caused by the measuring current. Although the particles of SMC materials have been coated by a thin electrical insulation, the eddy current might be non-negligible due to the possible insulation damage during the high pressure compaction process. Ideally, the measuring current should be as close to zero as possible but the reading error could be large.

7.3 Measurement of no-load core losses

The no-load core loss is measured by separating the core loss from the mechanical loss using the dummy stator method, which includes two measurements. In the first measurement, the prototype is driven by a DC motor and the power fed into the DC motor is measured. The second measurement is conducted while the SMC stator of the prototype is replaced by a wood tube.

The difference between the readings of electromagnetic power for the two cases gives the core loss. As illustrated in Fig. 11, the measurements validate the calculations. It is assumed that the core loss and mechanical loss of the DC driving motor are constant at certain rotor speed. The dummy stator is used to simulate the windage. The prototype is assumed to have

15

the same windage and friction loss for the SMC stator and the dummy stator if it is driven at the same speed.

8. Conclusion

This paper reports the computation of parameters of a claw pole PM motor with SMC stator core by using 3D magnetic field FEA. The winding flux, back *emf*, inductance and core loss are computed taking into account the effects of non-linearity of the core and armature reaction. The accurate determination of these parameters plays a key role in design and optimisation of high performance electrical machines, particularly when developing new machines with new materials and novel structures. The theoretical computations have been validated by the experimental results on the claw pole SMC motor prototype.

Reference:

[1] 'The latest development in soft magnetic composite technology'. Reports of Höganäs AB, Sweden, 1997-2005. Available at http://www.hoganas.com, see News then SMC update.

[2] Jack A.G.: 'Experience with the use of soft magnetic composites in electrical machines'. Int. Conf. on Electrical Machines, Istanbul, Turkey, Sept. 1998, pp. 1441-1448.

[3] Persson M., Jansson P., Jack A.G., and Mecrow B.C.: 'Soft magnetic composite materials – use for electrical machines'. 7th IEE Conf. on Electrical Machines and Drives, Durham, England, Sept. 1995, pp. 242-246.

[4] Guo Y.G., Zhu J.G., Watterson P.A., and Wu W.: 'Comparative study of 3-D flux electrical machines with soft magnetic composite core'. *IEEE Trans. Industry Applications*, 2003, **39**, (6), pp. 1696-1703.

[5] Guo Y.G., Zhu J.G., Zhong J.J., and Wu W.: 'Core losses in claw pole permanent magnet machines with soft magnetic composite stators'. *IEEE Trans. Magn.*, 2003, **39**, (5), pp. 3199-3201.

[6] Guo Y.G., Zhu J.G., Watterson P.A., and Wu W.: 'Development of a claw pole permanent magnet motor with soft magnetic composite stator'. *Australian J. Electrical & Electronic Eng.*, 2005, **2**, (1), pp. 21-30.

[7] Guo Y.G., Zhu J.G., and Zhong J.J., 'Measurement and modeling of magnetic properties of soft magnetic composite materials under 2D vector magnetizations', accepted for publication in the *Journal of Magnetism and Magnetic Materials*, 2006. In press. (Available online: http://authors.elsevier.com/sd/article/S0304885305008164)

[8] Upadhyay P.R., Rajagopal K.R., and Singh B.P.: 'Effect of armature reaction on the performance of an axial-field permanent-magnet brushless DC motor using FE method'. *IEEE Trans. Magn.*, 2004, **40**, (4), pp. 2023-2025.

[9] Demerdash N.A., and Nehl T.W.: 'Electrical machinery parameters and torques by current and energy perturbations from field computations – part I: theory and formulation'. *IEEE Trans. Energy Convers.*, 1999, **14**, (4), pp. 1507-1513.

[10] Demerdash N.A., and Nehl T.W.: 'Electrical machinery parameters and torques by current and energy perturbations from field computations – part II: applications and results'. *IEEE Trans. Energy Convers.*, 1999, **14**, (4), pp. 1514-1522.

[11] Gyimesi M., and Ostergaard D.: 'Inductance computation by incremental finite element analysis'. *IEEE Trans. Magn.*, **35**, (3), 1999, pp. 1119-1122.

[12] Guo Y.G., Zhu J.G., Lu H.W., Chandru R., Wang S.H., and Jin J.X.: 'Determination of winding inductance in a claw pole permanent magnet motor with soft magnetic composite core'. Australasian U. Power Eng. Conf., Hobart, Australia, Sept. 2005, pp. 659-664.

[13] Guo Y.G., Zhu J.G., Lin Z.W., and Zhong J.J.: 'Measurement and modeling of core losses of soft magnetic composites under 3D magnetic excitations in rotating motors'. *IEEE Tran. Magn.*, 2005, **41**, (10), pp. 3925-3927.

[14] Zhu J.G., 'Numerical modeling of magnetic materials for computer aided design of electromagnetic devices', Ph.D. thesis, University of Technology, Sydney, July 1994.
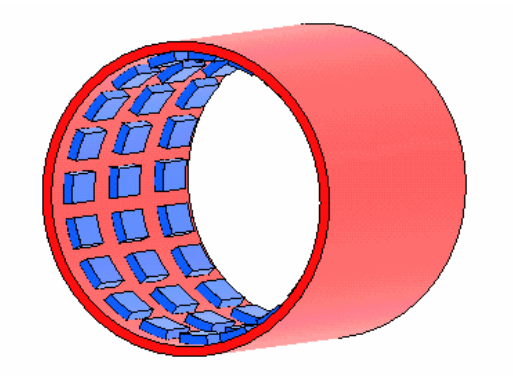
(a)
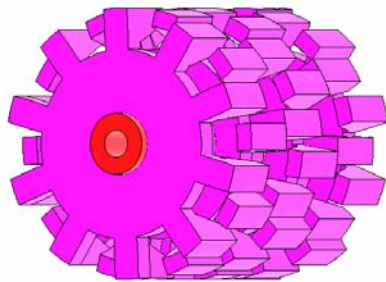
(b)

Fig. 1. Magnetically relevant parts of the claw pole SMC motor: (a) rotor, (b) stator.

Table I: Major dimensions and performance

Dimensions and performance	Quantities
Rated frequency (Hz)	300
Number of phases	3
Rated power (W)	500
Rated line-to-neutral voltage (V)	64
Rated phase current (A)	4.1
Rated speed (r/min)	1800
Rated torque (Nm)	2.65
Rated efficiency (%)	81
Rated temperature rise (^{o}C)	75
Number of poles	20
Stator core material	SOMALOY™ 500
Stator outer radius (mm)	40
Effective stator axial length (mm)	93
Rotor outer radius (mm)	47
Rotor inner radius (mm)	41
Permanent magnets	NdFeB, Grade N30M
Number of magnets	60
Magnet dimensions	OD88 x ID82 x 15 mm arc 12°
Magnetisation directions	Radially outward or inward
Main airgap length (mm)	1
Number of coils	3
Coil window dimension (mm^2)	17 x 11
Number of turns	75
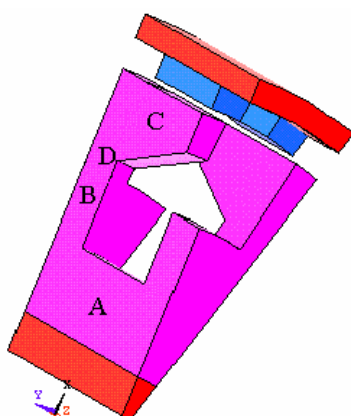
Fig. 2. FEA solution region
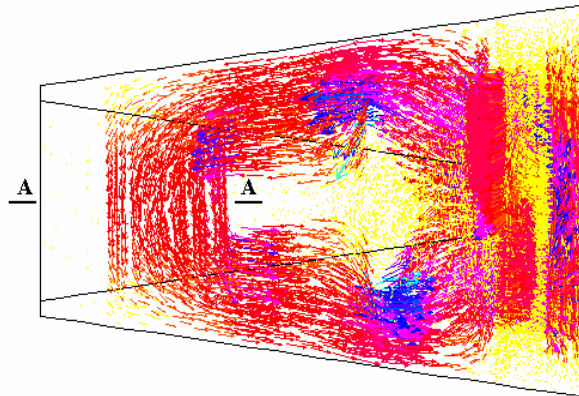
Fig. 3. Plots of flux density vectors generated by PMs only
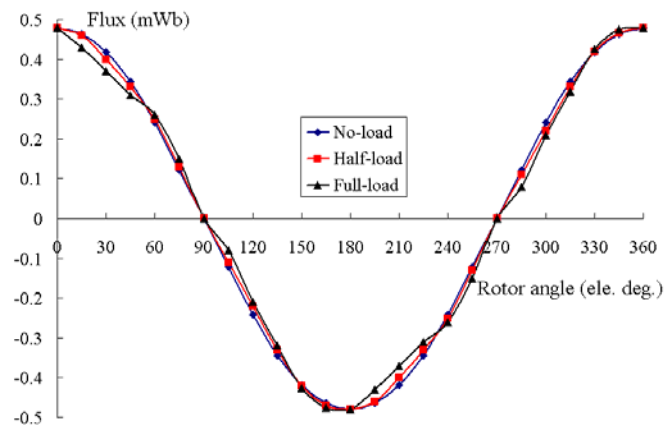
Fig. 4. Per-turn flux of a phase winding produced by PMs
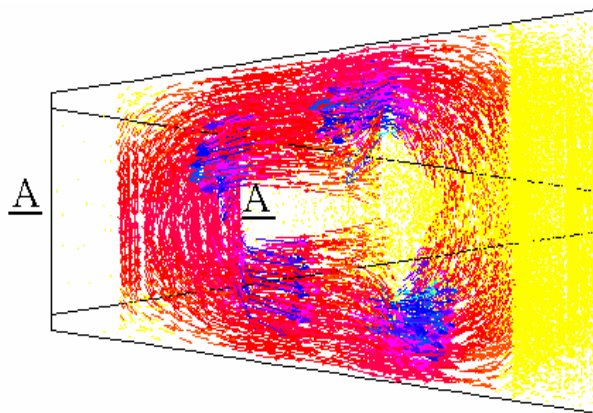
Fig. 5. Plots of flux density vectors generated by the stator current only
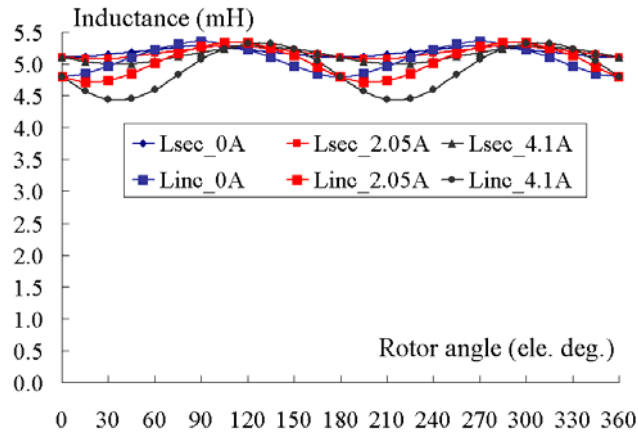
Fig. 6. Computed secant and incremental inductances
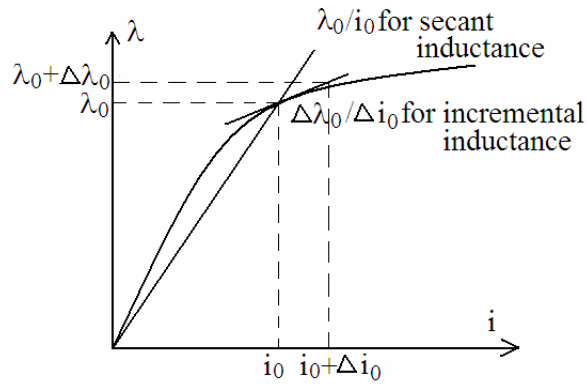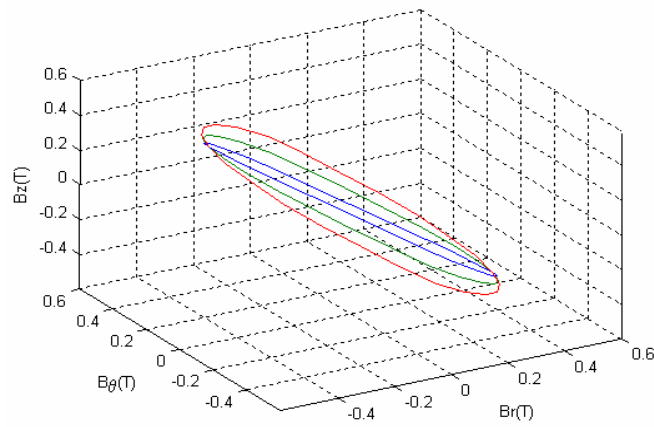

Fig. 7. Flux-linkage versus current

Fig. 8. Flux density loci at Point C of Fig. 2: inside locus for no-load, middle one for half-load, and outside one for full-load
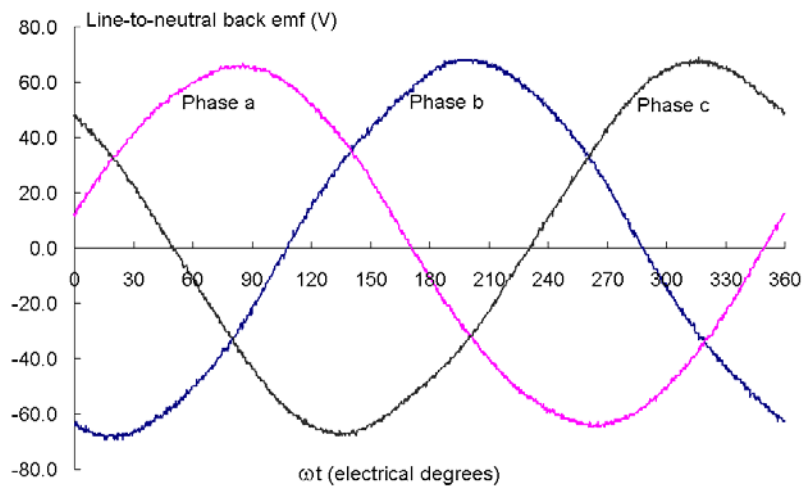
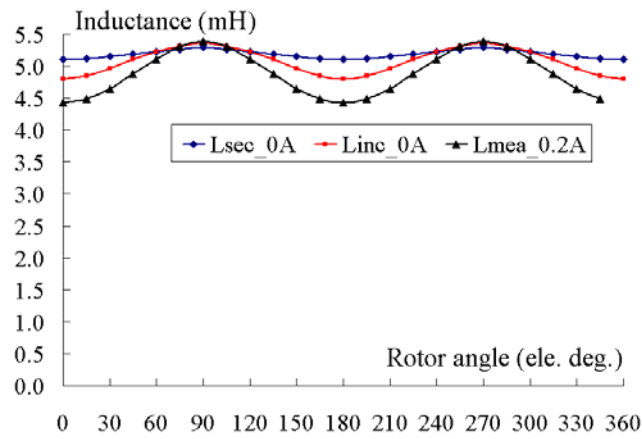Fig. 9. Measured *emf* waveforms at 1800 rpm
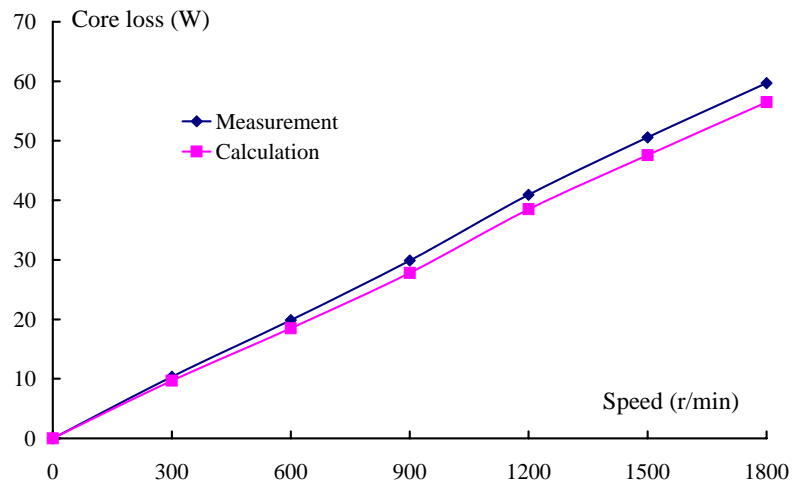

Fig. 10. Computed and measured inductances

Fig. 11. Core loss calculation and measurement at no-load